

Special  
Collection

# Solid-Phase Lipase-CuNPs Biohybrids as Catalysts for One-Pot Parallel Synthesis of 2,3,4-Triacetyl-D-Gluconic Acid

Noelia Losada-García,<sup>[a]</sup> Esteban P. Urriolabeitia,<sup>[b]</sup> and Jose M. Palomo\*<sup>[a]</sup>

Solid-phase lipase/metal nanobiohybrids, generated by growth of copper nanoparticles on enzyme matrixes immobilized on graphene, were used as heterogeneous catalysts with dual-activity for the regioselective production of 2,3,4-triacetyl-D-gluconic acid from  $\alpha$ -peracetylated-glucose in a one-pot parallel process combining a lipase-mediated regioselective hydrolytic monodeprotection with a metal-catalyzed oxidation in aqueous media. A novel synthetic strategy, based on the *in situ* fabrication of Cu nanoparticles induced by lipase molecules specifically immobilized on a multi-layer graphene material by interfacial adsorption fixing them in the active open conformation, has been described. *Thermomyces lanuginosus* lipase was firstly used to prepare the functionalized multi-layer graphene

from graphite as a biographene preparation (Biographene, BIOG), support used to successfully immobilize *Candida rugosa* lipase (CRL). This immobilized form BIOG-CRL was further used to create successful active bifunctional enzyme-metal nano-architectures. Two different Cu-lipase hybrids were synthesised, where Cu species and nanoparticles size were different depending on the methodology. Regioselectivity and stability of the hybrids were evaluated successfully in the production of monosaccharide building blocks, besides the robustness of the hybrids in recyclability experiments. These findings highlight the potential of these solid-phase nanoarchitectures as useful tools in the synthesis of complex glycoderivatives for use in food, medicine, and cosmetics.

## Introduction

Glycans derivatives are extremely important molecules in key biological processes. They are involved in regio- and stereochemical controlled fabrication of glycosylated molecules, as drug and vaccines, but also in fabrication of early diagnosis and more effective and targeted therapeutic tools.<sup>[1–5]</sup> In this respect, one of the most difficult entities is the fabrication of partially protected sugars (monosaccharides) with orthogonal functional groups as key intermediates, which required extremely time-consuming processes with multiple steps and specific purification steps, finally resulting in moderate or low yields of target product at the end.<sup>[6]</sup>

In particular, gluconic acid and its derivatives have been applied globally with different shares in the construction (45%), food (35%), medicine (10%) and other (10%) industries. Several

features made them very attractive in commercial applications. For example, gluconic acid is a versatile organic acid, which is noncorrosive, mildly acidic, non-irritating, odourless, non-toxic, and easily degradable. As a food additive under the laws of some countries, gluconic acid and derivatives are commonly added to dairy products, beverages and bakery to maintain flavour and prevent precipitation.<sup>[7]</sup>

The development of cascade or parallel reaction systems represents the perfect strategy to produce these semiprotected monosaccharides, as they display several advantages compared to a typical single reaction, such as atom economy, step-saving, and high yield, therefore providing high efficiency to the chemical process.<sup>[8–11]</sup>

In particular, regioselective biocatalytic strategies and metal-catalysis have been successfully applied in carbohydrate chemistry,<sup>[12]</sup> thus a combination of both would be an ideal task, low exploited until now.<sup>[13]</sup> However, a proper design of enzyme-metal combination is challenging, because these two types of catalysts often deactivate mutually and the reaction conditions for one cannot be applied to the other.<sup>[14]</sup>

Even more, although different strategies have been developed in the recent years to create metalloenzymes, all of them show some sort of problems. For instance, organometallic complexes were inserted in the enzyme cavity, eliminating the enzymatic activity.<sup>[15–17]</sup> In the same respect, both, metallic and enzymatic, catalysts were immobilized on functionalized porous-support in separate way,<sup>[17]</sup> which still represent a drawback in some cases in term of cascade reactions for example due to low reactivity of the heterogeneous phase under ambient conditions and poor molecular transport.<sup>[18]</sup>

Few years ago, novel interesting strategies to drawback some limitations to successfully performed tandem and cascade reactions have been developed.<sup>[19–22]</sup> Indeed our research group

[a] N. Losada-García, J. M. Palomo  
Instituto de Catálisis y Petroleoquímica (ICP), CSIC  
C/Marie Curie 2  
28049 Madrid (Spain)  
E-mail: josempalomo@icp.csic.es

[b] E. P. Urriolabeitia  
Instituto de Síntesis Química y Catálisis Homogénea (ISQCH)  
CSIC-Universidad de Zaragoza  
Pedro Cerbuna 12  
50009 Zaragoza (Spain)

Supporting information for this article is available on the WWW under <https://doi.org/10.1002/cctc.202201632>

This publication is part of a Special Collection on "Heterogeneous Chemo-Enzymatic Catalysis". Please check the ChemCatChem homepage for more articles in the collection.

© 2023 The Authors. ChemCatChem published by Wiley-VCH GmbH. This is an open access article under the terms of the Creative Commons Attribution Non-Commercial License, which permits use, distribution and reproduction in any medium, provided the original work is properly cited and is not used for commercial purposes.

developed a strategy to synthesize metal nanoparticles induced by enzymes, creating a hybrid system constituted by an enzyme network with embedded homogeneously dispersed and stabilized metal nanoparticles directly in aqueous media at room temperature.<sup>[23–27]</sup> This represented an interesting method for intramolecular catalytic processes. However, in the synthetic Cu-enzyme hybrids, the remaining enzymatic activity of these nanobiohybrids after synthesis was partial or totally reduced,<sup>[28]</sup> limiting their application in cascade processes. Cu-hybrids have been described as quite interesting, cheap and environmentally friendly catalysts in oxidation processes.<sup>[28]</sup>

Therefore, a strategy directed to maintain the full enzymatic activity, together with the metallic one, is mandatory. In particular, the use of lipases, especially *Candida rugosa* lipase (CRL), has shown excellent regioselectivity in monodeprotection of sugars.<sup>[29]</sup> In order to establish a bi-functional catalyst to conserve the activity and the excellent regioselectivity, the site-specific and selective immobilization of these enzymes on solid supports in an active and stable form could fulfil this drawback. In particular, the immobilization of lipases on hydrophobic supports allow to fixing exclusively the active open conformation of the enzyme.<sup>[30]</sup>

This phenomenon could allow to synthesize *in situ* nanoparticles, exclusively on the protein matrix, in such a way that more metal surface and more active sites could be available for catalytic performance.

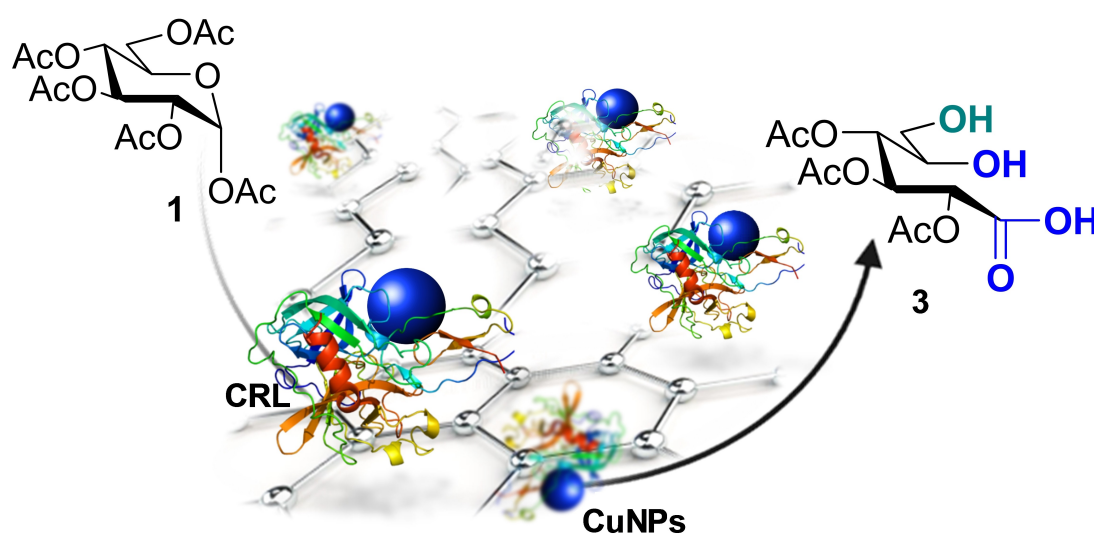
Herein, we report the design and synthesis, for the first time, of a new type of bifunctional hybrid heterogeneous catalysts, CRL–Cu nanoparticles immobilized derivatives on enzyme-exfoliated graphene (biographene) and their successfully use in the one-pot regioselective synthesis of 2,3,4-triacetyl-D-gluconic acid from peracetylated- $\alpha$ -glucose in aqueous media at room temperature in high yields (Scheme 1).

## Results and Discussion

First, the CRL immobilization was attempted. For that, our recently reported strategy<sup>[33]</sup> to direct bio-exfoliation of graphite for obtaining lipase immobilized graphene derivatives was applied using CRL instead of *Thermomyces lanuginosus* lipase (TLL). However, a very low exfoliation capacity was observed using this lipase, with less than 10% of CRL immobilized. Therefore, the first step was the bioexfoliation of graphite by mechanical sonication and then directly adsorption of TLL, creating the functionalized graphene of 5–6 layers (called BIOG).<sup>[33]</sup> Considering that, the strategy was to use BIOG as support for CRL immobilization. In this way, more than 99% offered enzyme (10 mg/g support loading) was site-specific immobilized (BIOG-CRL) (Figure 1a) whereas 50% was observed when 20 mg of enzyme was offered per gram of support (Figure S1). This demonstrated that CRL seems to be too large for exfoliation (63 kDa compared to 33 kDa of TLL) but it is able to interact by interfacial adsorption with graphene previously exfoliated, site-oriented interactions between hydrophobic graphene surface with particularly hydrophobic pocket area in the open conformation of lipase constitute by surrounding active site and lid area (Figure S1). Therefore, TLL immobilization in the formation of BIOG ensures the presence of lipase (CRL) by fixing the open conformation and homogeneously dispersed on the solid material.

For preparation of the bifunctional catalysts, BIOG-CRL was added to phosphate buffer solution containing copper sulphate salt after incubation for 16 h. Two different strategies were used, directly in phosphate buffer (pH = 7), and without or with an additional reducing step with NaBH<sub>4</sub> for 30 min, producing the heterogeneous hybrids BIOG-CRL-CuNPs-1 and BIOG-CRL-CuNPs-2, respectively (Figure 1).

Then, structural characterization of the hybrids was performed (Figures 2–3, S2). In the case of BIOG-CRL-CuNPs-1, the



**Scheme 1.** One-pot regioselective synthesis of 2,3,4-triacetyl-D-gluconic acid catalyzed by novel biographene-CRL-CuNPs bifunctional hybrid.

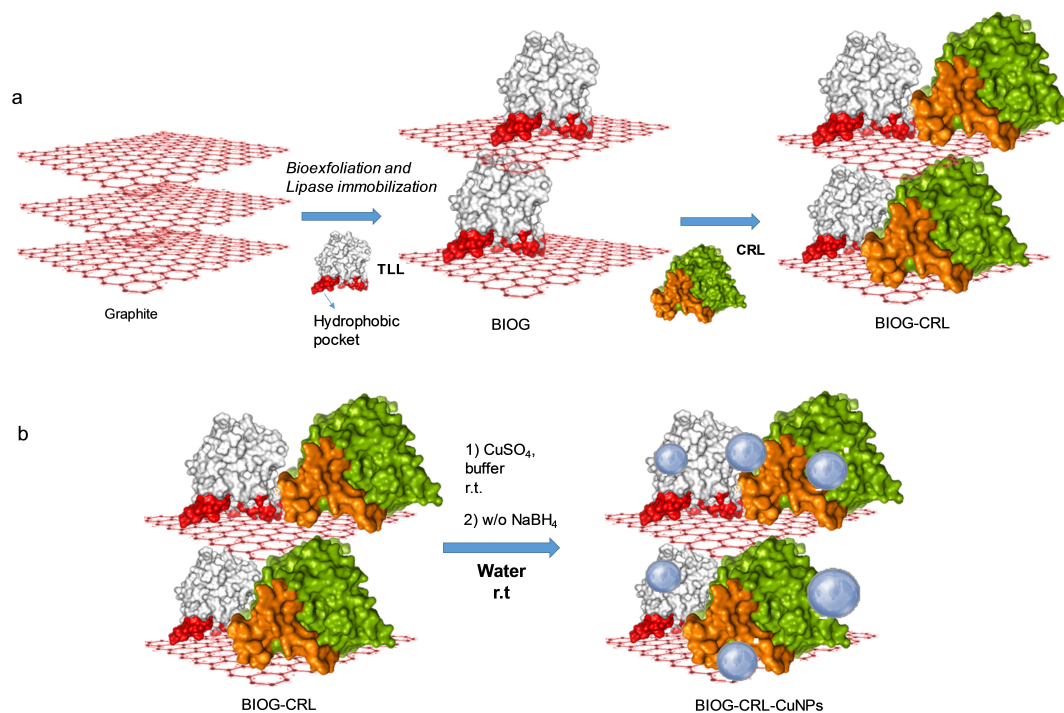


**Figure 1.** Preparation and formation mechanism of BIOG-CRL-CuNPs hybrids. a) Immobilization scheme of CRL into BIOG. b) CuNPs formation into BIOG-CRL.

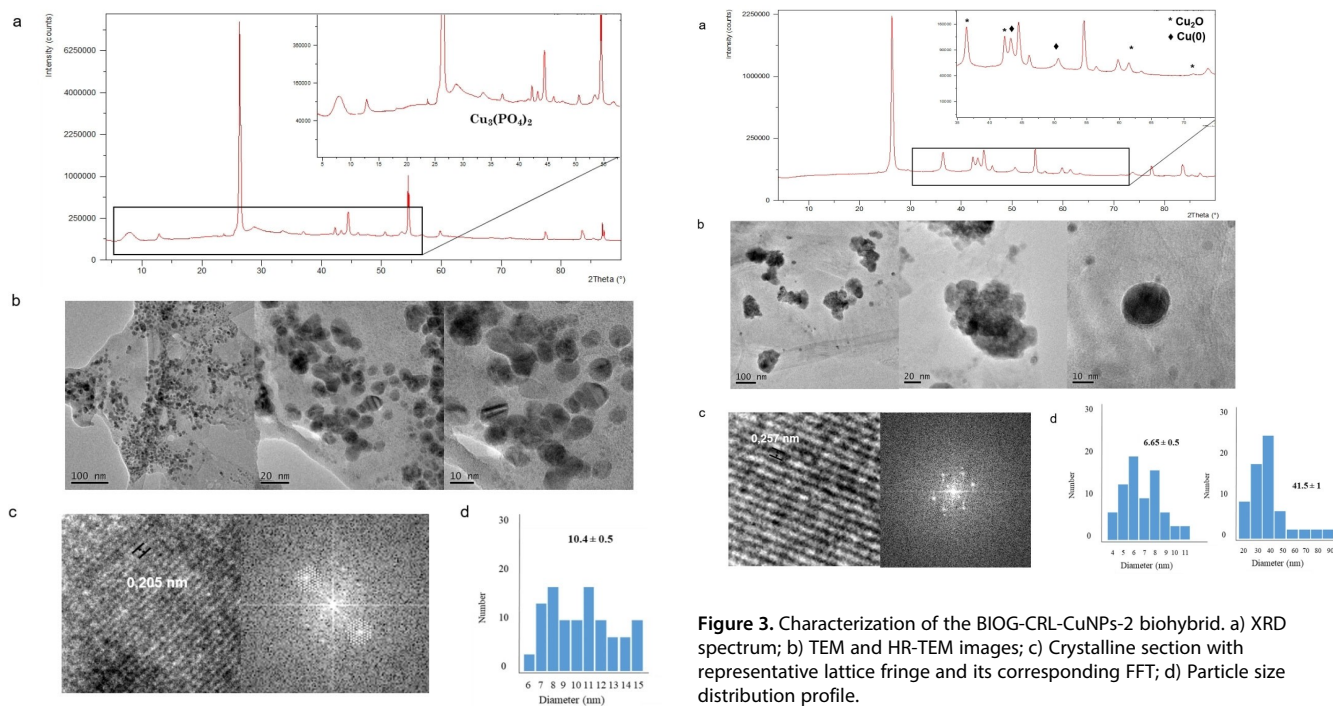


**Figure 2.** Characterization of the BIOG-CRL-CuNPs-1 biohybrid. a) XRD spectrum; b) TEM and HR-TEM images; c) Crystalline section with representative lattice fringe and its corresponding FFT; d) Particle diameter size distribution profile.

**Figure 3.** Characterization of the BIOG-CRL-CuNPs-2 biohybrid. a) XRD spectrum; b) TEM and HR-TEM images; c) Crystalline section with representative lattice fringe and its corresponding FFT; d) Particle size distribution profile.

wide-angle X-ray diffraction (XRD) and X-ray photoelectron analysis (XPS) analysis confirmed the presence of  $\text{Cu}_3(\text{PO}_4)_2$  as unique copper species (Figure 2a and Figure S2).

Transmission electron microscopy (TEM) analysis revealed mainly the formation of small crystalline spherical nanoparticles with an average diameter size of  $10.4 \pm 0.5$  nm (Figure 2b–d).

The inductively coupled plasma-optical emission spectroscopy results showed that the content of Cu was 8% (w/w).

In the case of BIOG-CRL-CuNPs-2 (Figure 3), the XRD revealed the formation of different species, confirming the presence of Cu<sub>2</sub>O as Cu species in this hybrid, by observation of four characteristic peaks, three of them assigned to planes (111), (200) and (220), respectively, of the fcc Cu lattice, with a fraction of Cu (0) (Figure 3a). XPS analysis confirmed the formation of copper species (Figure S3). TEM analyses revealed the formation of aggregated clusters of highly crystalline nanoparticles with average size of 41 nm with a minor fraction of spherical nanoparticles of average diameter size of around 7 nm (Figures 3b–d). In this case the content of Cu was of 9% determined by ICP-OES.

Both protocols were repeated using BIOG, and therefore, only TLL as protein scaffold for the bifunctional hybrid formation was used, obtaining hybrids BIOG-CuNPs-1 and BIOG-CuNPs-2, respectively (Figures S4–5). In both cases, content of Cu was slightly lower, approx. 6.5%, although the size of nanoparticles formed in the biohybrids was larger. In particular, this effect was more important in the comparison between BIOG-CuNPs-2 and BIOG-CRL-CuNPs-2, which could be due to a better stability of the graphene layers in the reducing step with borohydride at pH 7 by the presence of both proteins (covering more support surface area).

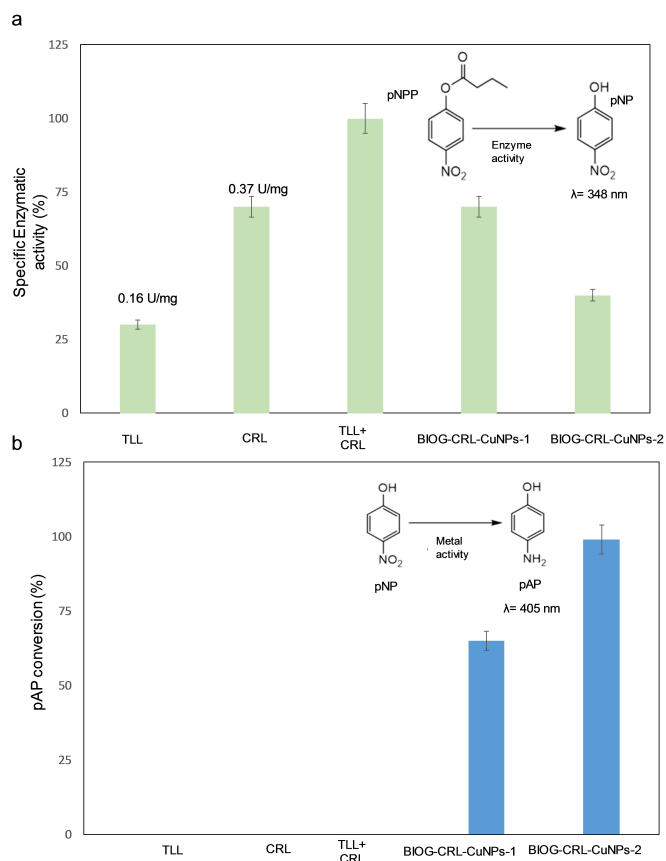
In order to demonstrate that the copper nanoparticles were synthesized exclusively induced by the enzyme, and only on the protein structure, BIOG or BIOG-CRL was chemically modified with polyethyleneimine (Mw800), blocking all accessible carboxylic groups in the protein (where metal is coordinated before nanoparticle is formed). Negligible amount of copper was detected in any case, confirmed by X-ray and mass analysis (data not shown).

Then, enzymatic and metallic activities of the bifunctional catalysts were evaluated. For the enzymatic activity, the hydrolysis of p-nitrophenyl propionate as model reaction was attempted (Figure 4a). As we previously observed with other enzymes,<sup>[28]</sup> copper hybrids synthesized using unsupported lipases were performed and no enzymatic activity was detected (data not shown).

Both enzymes on BIOG-CRL (TLL as support scaffold and CRL) showed hydrolase activity against this substrate, and BIOG-CRL showed a hyperactivation of two times (Figure S1). After the synthetic nanoparticle formation, BIOG-CRL-CuNPs-1 conserved 70% of the full initial enzymatic activity (considering both lipases activity) whereas BIOG-CRL-CuNPs-2 exhibited around 40% of the initial total enzyme activity against pNPP (Figure 4a). In the hybrids synthesized using BIOG, the complete enzymatic activity was conserved (Figure S6).

For evaluating the metallic activity, a reducing reaction of pNP to p-aminophenol (pAP) was used (Figure 4b). BIOG-CRL-CuNPs-2 as Cu(I) catalyst showed the best performance, with >99% conversion after 10 min incubation. BIOG-CRL-CuNPs-1 showed lower activity, with around 65% conversion at the same time. Soluble enzymes or corresponding immobilized derivatives (BIOG, BIOG-CRL) did not show any metallic activity (Figure 4).

In order to evaluate the potential application of these heterogeneous biohybrids as bifunctional catalysts in single compartment, the one-pot transformation of pNPP to pAP

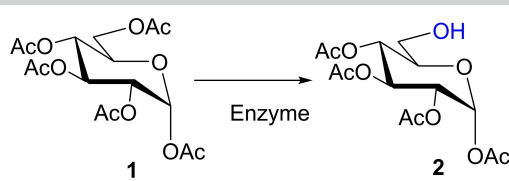


**Figure 4.** a) Specific enzymatic activity of the different BIOG-CRL-CuNPs hybrids. Experimental conditions: pNPP (0.4 mM), sodium phosphate buffer (5 mL, 25 mM, pH 7), 3 mg solid catalyst or 20  $\mu$ l of free enzyme, 25 °C. b) Metallic activity of different BIOG-CRL-CuNPs hybrids in reduction of pNP to pAP. Conditions: p-Nitrophenol (pNP), 40 mM NaBH<sub>4</sub>, 2 mL of distilled water, 10 mg of catalyst, air and room temperature.

(enzymatic + metallic) in distilled water at room temperature was tested (Figure S7). Both lipases in solution or even the immobilized form BIOG or BIOG-CRL were tested and no final conversion of pAP was obtained after 120 h incubation. For the biohybrids, BIOG-CRL-CuNPs-1 complete the cascade producing >99% of pAP after 60 min incubation and BIOG-CRL-CuNPs-2 was effective in the cascade although needed 120 minutes to complete the process. In this cascade, the limiting step is the enzymatic one, which makes the difference between the respective efficiencies; that is, the differences in reaction times is due solely to the enzymatic step (Figure 4).

Once the dual activity of the bifunctional hybrids was confirmed, these new CRL/Cu biohybrid catalysts were applied in the chemoenzymatic synthesis of an important high-added value carbohydrate building block, by an enzymatic hydrolytic step coupled with a selective oxidative process catalysed by Cu.

First, the activity of the hybrids was evaluated in the two reactions separately. The enzymatic activity was evaluated in the regioselective monodeprotection of peracetylated- $\alpha$ -glucose (1) in aqueous media at room temperature (Table 1). In this case only the enzymatic step will be due to the CRL activity, because TLL did not catalyse the hydrolysis of 1,<sup>[30]</sup> thus only BIOG-CRL preparations

**Table 1.** Regioselective hydrolysis of  $\alpha$ -D-glucose pentacetate (**1**) catalysed by BIOG-CRL-CuNPs hybrids.<sup>[a]</sup>


| Entry | Catalyst         | Time [h] | <b>2</b> [%] |
|-------|------------------|----------|--------------|
| 1     | CRL-CuNPs        | 96       | 0            |
| 2     | BIOG             | 96       | 0            |
| 3     | BIOG-CRL         | 96       | > 99         |
| 4     | BIOG-CuNPs-1     | 96       | 0            |
| 5     | BIOG-CuNPs-2     | 96       | 0            |
| 6     | BIOG-CRL-CuNPs-1 | 96       | > 99         |
| 7     | BIOG-CRL-CuNPs-2 | 96       | > 99         |

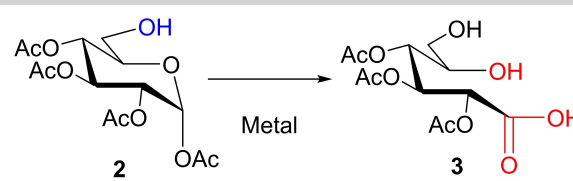
[a] Conditions: **1** (5 mg), sodium acetate buffer at pH 4.8 (50 mM, 2 mL), ACN (20%), catalyst (150 mg). r.t: room temperature (c.a. 20°C); Conversion of the product was measured by TLC and HPLC. TLC conditions were hexane: ethyl acetate (1:1) solution. The HPLC conditions were an isocratic mixture of 70:30 water: ACN as mobile phase, UV detection at 215 nm, and a flow rate of 1 mL/min.

showed activity (Table 1). The preparation using soluble enzyme, CRL-CuNPs, which did not show enzymatic activity against pNPP, was tested in this hydrolysis and no conversion was observed (Table 1, entry 1). BIOG-CRL showed high regioselectivity, producing >99% of 6-OH monodeprotected product **2** (>95% isolated yield) after 96 hours (Table 1, entry 3). Both BIOG-CRL-CuNPs hybrids showed similar regioselective result (Table 1, entries 6–7), demonstrating that the enzymatic activity was fully conserved after CuNPs formation in both cases.

Regioselective hydrolysis of alpha-peracetylated-galactose or mannose<sup>[30]</sup> were also investigated using BIOG-CRL-CuNPs catalysts, but no regioselectivity was found (data not shown).

Starting from **2**, the metallic-activity of the different Cu hybrids was tested in a specific oxidation step (Table 2). The hybrids showed different efficiency depending on the Cu species and size. The different catalysts were tested in absence or in the presence of H<sub>2</sub>O<sub>2</sub>. We have demonstrated the efficiency of the Cu in different process catalysed in the presence of H<sub>2</sub>O<sub>2</sub>.<sup>[28]</sup> BIOG and BIOG-CRL did not show any oxidative process, even in the presence of hydrogen peroxide (Table 2, entries 1–2, 5–6). The bifunctional CRL-Cu catalysts did not show any activity in absence of hydrogen peroxide (Table 2, entries 3–4), however, a new product was obtained in the presence of 500 mM of hydrogen peroxide. BIOG-CRL-CuNPs-1 showed the best result in the synthesis of product **3** with >99% conversion after 72 h whereas BIOG-CRL-CuNPs-2 exhibited 50% conversion after 120 h. These results show that smaller Cu(II) nanoparticles (in BIOG-CRL-CuNPs-1) were more efficient than Cu(I) nanoparticles, respectively. The product obtained in this reaction was isolated and characterized by NMR as the triacetylated-gluconic acid derivative **3** (Figures S8–S10).

After the control experiments, the reaction starting from **1** was attempted (Figure 5). BIOG-CRL-CuNPs-1 was able to transform **1** to **3** in yield >95% after 72 h, while BIOG-CRL-CuNPs-2 showed,

**Table 2.** Regioselective oxidation of  $\alpha$ -6-OH (**2**) catalysed by BIOG-CRL-CuNPs hybrids.<sup>[a]</sup>


| Entry | Catalyst         | H <sub>2</sub> O <sub>2</sub> [mM] | Time [h] | <b>3</b> [%] |
|-------|------------------|------------------------------------|----------|--------------|
| 1     | BIOG             | 0                                  | 120      | 0            |
| 2     | BIOG-CRL         | 0                                  | 120      | 0            |
| 3     | BIOG-CRL-CuNPs-1 | 0                                  | 120      | 0            |
| 4     | BIOG-CRL-CuNPs-2 | 0                                  | 120      | 0            |
| 5     | BIOG             | 500                                | 120      | 0            |
| 6     | BIOG-CRL         | 500                                | 120      | 0            |
| 7     | BIOG-CRL-CuNPs-1 | 500                                | 72       | > 99         |
| 8     | BIOG-CRL-CuNPs-2 | 500                                | 120      | 50           |

[a] Conditions: **2** (5 mg), sodium acetate buffer at pH 4.8 (50 mM, 2 mL), ACN (20%), H<sub>2</sub>O<sub>2</sub>, catalyst (50 mg). r.t: room temperature (c.a. 20°C); Conversion of the product was measured by TLC and HPLC. TLC conditions were hexane: ethyl acetate (1:1) solution. The HPLC conditions were an isocratic mixture of 70:30 water:ACN as mobile phase, UV detection at 215 nm, and a flow rate of 1 mL/min.

as previously in the metallic step, a lower efficiency, with only 50% yield after this incubation time (Figure 5b). The oxidation process was clearly caused by the Cu, BIOG-CRL did not produce any amount of **3**.

Therefore, the benefit of the presence of both catalysts in the same compartment in the parallel reaction was demonstrated, being faster than processes separately. The applicability of BIOG-CRL-CuNPs-1 was evaluated in a recycling experiment. After 5 cycles at optimal condition, the catalyst conserved >95% efficiency in the catalytic process (Figure 5c).

## Conclusion

Novel bifunctional heterogeneous lipase-CuNPs hybrid catalysts were synthesized. Lipase from *C. rugosa*, specific enzyme in regioselective monodeprotection of sugars, was immobilized on a biographene preparation, and this immobilized preparation was used as solid-phase scaffold to the *in situ* fabrication of Cu nanoparticles induced by lipases molecules creating successful enzyme-metal nanoarchitectures. Two different Cu-hybrids were obtained, where Cu<sub>3</sub>(PO<sub>4</sub>)<sub>2</sub> nanoparticles (BIOG-CRL-CuNPs-1) of around 10 nm or Cu<sub>2</sub>O nanoparticles around 41 nm (BIOG-CRL-CuNPs-2) were produced. The participation from different chemo- and biocatalytic components of them was firstly demonstrated in the domino cascade process to finally applied to the target molecule, transforming  $\alpha$ -peracetylated glucose to 2,3,4-triacetyl-D-gluconic acid, by lipase-mediated regioselective hydrolytic monodeprotection and metal-catalyzed oxidation in aqueous media. This parallel reaction although works using both catalysts, was more efficient by using BIOG-CRL-CuNPs-1, with a complete conversion after 72 h. Furthermore, recycling studies demon-

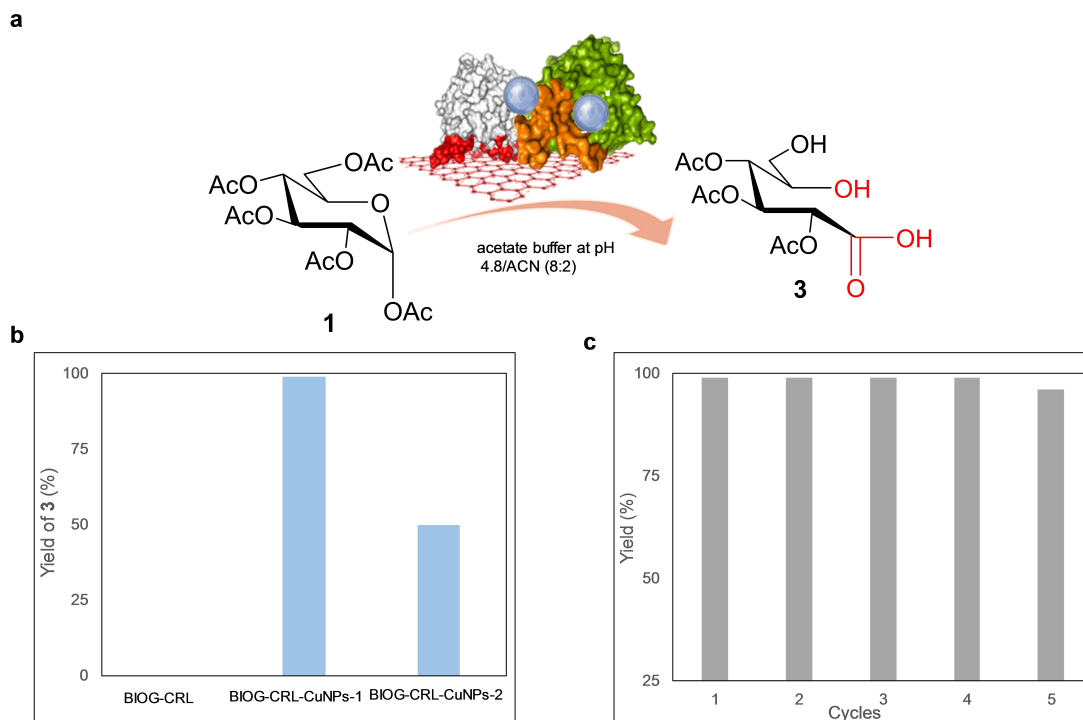


**Figure 5.** Direct parallel reaction from **1** to produce regioselectively **3** catalyzed by Cu-hybrids. a) Chemoenzymatic scheme, b) Conversion of **3** by the different hybrids after 72 h reaction in the presence of 500 mM of H<sub>2</sub>O<sub>2</sub>. c) Reaction yield of five cycles using BIOG-CRL-CuNPs-1 in the conversion of **1** to **3**.

strated the high robustness of these systems, maintaining more than 95% activity after 5 cycles of used.

These excellent results open the potential application as catalytic platform for other complex pharmaceutical synthesis and in the field of biomedicine and biotechnology. Indeed, sustainable synthetic application in the fabrication of building blocks with orthogonal functional molecules are mandatory in the preparation of novel glycoderivatives, such as oligosaccharides with interesting biological activities, such as microbiota prebiotic properties, improving health of skin or even novel antiviral molecules.

## Experimental Section

### Materials

Lipase from *Thermomyces lanuginosus* solution (Lipozyme® TL 100L) was purchased from Novozymes (Copenhagen, Denmark). Copper (II) sulfate pentahydrate [Cu<sub>2</sub>SO<sub>4</sub>·5H<sub>2</sub>O], ethyl acetate, sodium acetate, sulphuric acid (96%) and hydrogen peroxide (33%) were from Panreac (Barcelona, Spain). Graphite flakes, p-nitrophenol, p-nitrophenyl propionate, p-aminophenol, sodium bicarbonate, sodium phosphate, toluene, sodium borohydride, Triton-X100, lipase from *Candida rugosa*, α-D-glucose pentaacetate (99%) were purchased from Merck (Darmstadt, Germany). HPLC grade acetonitrile was from Scharlau (Barcelona, Spain).

### Structural characterization

The metal contents were measured by an inductively coupled plasma - optical emission spectrometer (ICP-OES) (OPTIMA 2100 DV instrument; PerkinElmer, Waltham, MA, USA). X-Ray diffraction (XRD) patterns with Cu Kα radiation (Texture Analysis D8 Advance Diffractometer; Bruker, Billerica, MA, USA) were used for structure characterization. Transmission electron microscopy (TEM) and high-resolution TEM microscopy (HR-TEM) images (2100F microscope; JEOL, Tokyo, Japan) were used to measure the size and distribution of the samples. Interplanar spacing in the nanostructures was calculated by using the inverted Fourier transform with the GATAN digital micrograph program (Corporate Headquarters, Pleasanton, CA, USA). X-ray photoelectron analysis (XPS) was carried out on SPECS GmbH spectrometer equipped with Phoibos 150 9MCD energy analyzer. A nonmonochromatic magnesium X-ray source with a power of 200 W and voltage of 12 kV was used. To recover the nanobiohybrids, a Biocen 22 R (Orto-Alresa, Ajalvir, Spain) refrigerated centrifuge was used. Spectrophotometric analyses were run on a V-730 spectrophotometer (JASCO, Tokyo, Japan). A HPLC pump PU-4180 and a UV-4075 UV-Vis detector (JASCO, Tokyo, Japan) was used to analyse the reactions. The reaction was followed by thin layer chromatography (TLC) (Merck silica gel 60 F254, Germany) and UV Spectroline lamp (Merck, Germany).

### NMR characterization

<sup>1</sup>H spectra were recorded in D<sub>2</sub>O solutions at 25 °C on a Bruker AV400 spectrometer (δ in ppm, J in Hz) at <sup>1</sup>H operating frequency of 400.13 MHz. The <sup>1</sup>H NMR spectra were referenced using the solvent signal as internal standard. The assignment of <sup>1</sup>H NMR peaks has been performed through standard 2D <sup>1</sup>H-COSY experiments (2 K points in t<sub>2</sub> using a spectral width of 12 ppm; 128 t<sub>1</sub>,

experiments were recorded and zero-filled to 1 K; for each  $t_1$  value two scans were signal-averaged using a recycle delay of 1 s). The  $^{13}\text{C}$  NMR peaks were identified using standard  $^1\text{H}$ - $^{13}\text{C}$  edited-HSQC and  $^1\text{H}$ - $^{13}\text{C}$  HMBC 2D-experiments. In both cases 4 K points in  $t_2$  using spectral widths of 12 ppm ( $^1\text{H}$ ) and 200 ppm ( $^{13}\text{C}$ ) were used, with averaged values of the coupling constants  $^1J_{\text{CH}} = 145$  Hz and long-range  $^nJ_{\text{CH}} = 10$  Hz. Typically, 128  $t_1$  experiments were recorded and zero-filled to 1 K. For each  $t_1$  value 16 (HSQC) or 64 (HMBC) scans were signal-averaged using a recycle delay of 1 s. ESI (ESI $^{+}$ ) mass spectra were recorded using an Esquire 3000 ion-trap mass spectrometer (Bruker Daltonic GmbH) equipped with a standard ESI/APCI source. Samples were introduced by direct infusion with a syringe pump. Nitrogen served both as the nebulizer gas and the dry gas. MALDI mass spectra were recorded using a Bruker MicroFlexTM or a Bruker AutoFlexTM III spectrometer, equipped with a time-of-flight mass analyzer, and using DIT (dithranol) as matrix. The HRMS mass spectra were recorded using a MicroToF Q, API-Q-ToF ESI with a mass range from 20 to 3000 m/z and mass resolution 15000 (FWHM).

### Exfoliation of graphite flakes using TLL (BIOG)

The graphite flakes (1 g) were added together with 20 mL of distilled water to a 50 mL centrifuge tube (50 mL Falcon tube). Once this was done, the graphite was exfoliated by alternating cycles of 5 min sonication/rest, for 1 h at an amplitude of 80%. To avoid excessive heating of the mixture, the 50 mL Falcon tube was introduced into a mixture of ice and cold acetone. This exfoliation allowed the weakening of the bonds between sheets. After that, commercial lipase solution of TLL, in both cases offering 5 mg lipase, were directly added to that and allowed to stir for a period of time between 1 h and 30 min, respectively. The selective adsorption of the lipase was followed by measuring the supernatant using the pNPP activity assay (described below). After lipase immobilization, the suspension turned cloudy black. Then, the mixture was transferred to 15 mL Falcon centrifuge tubes and centrifuged at 400 rpm for 1 min to remove some non-exfoliated graphite. After that, the black suspension was centrifuged at 8000 rpm for 10 min and then the water was removed. One mL of acetone was added to dissolve the black powder and then this mixture was transferred to a Petri dish and dried at 50 °C for 4 h. The method allowed to obtain BIOG with 6.3 mg<sub>protein</sub>/g<sub>support</sub> (final exfoliation yield: 80%).

### Preparation of CRL-graphene (BIOG-CRL)

One gram of graphite flakes was added together with 20 mL of distilled water to a 50 mL centrifuge tube. Once this was done, the graphite was exfoliated by alternating cycles of 5 min sonication/rest, for 1 h at an amplitude of 80%. To avoid excessive heating of the mixture, the 50 mL Falcon tube was introduced into a mixture of ice and cold acetone. After that, 5 mg of commercial lipase solution of TLL were directly added to that and allowed to stir for a period of time between 1 h. After lipase immobilization, the solid was separated from the supernatant and 20 mg of *Candida rugosa lipase* (CRL) in 20 mL of 25 mM sodium phosphate buffer pH 7 were added to the solid, leaving it on a roller. It was incubated for 2 h. Finally, it was centrifuged and dried at 50 °C for 4 h. The method allowed obtaining 800 mg of BIOG-CRL with 10 mg of CRL. This support contains 19 mg<sub>protein</sub>/g<sub>support</sub> (6.3 mg of TLL and 12.7 mg of CRL).

### General synthesis of BIOG-CRL-CuNPs hybrids

500 mg of BIOG-CRL were added to 20 mL buffer sodium phosphate 0.1 M pH 7 in a 50 mL glass vial containing a small

magnetic bar stirrer. Then, 200 mg of  $\text{Cu}_2\text{SO}_4 \cdot 5\text{H}_2\text{O}$  (10 mg/mL) were added to the solution with the support and it was maintained for 16 hours. After 16 h, the sediment generated was re-suspended in 5 mL of water. It was centrifuged again at 8000 rpm for 20 min and the supernatant was removed. The process was repeated two more times. Finally, the supernatant was removed and the pellet was resuspended in 2 mL of water and added to a cryogenization tube, frozen with liquid nitrogen and lyophilized overnight. After that, the so-called BIOG-CRL-CuNPs-1 was obtained.

Same procedure was repeated but after 16 h incubation, an additional reduction step was done adding 2 mL of  $\text{NaBH}_4$  (112 mg) aqueous solution (1.2 M) to the mixture, obtaining a final concentration of 0.12 M sodium borohydride, and reduced for 30 min. After that washing process and lyophilization was repeated as previously to finally obtain incubation, the mixture was centrifuged at 8000 rpm for 20 min. Another variation of the protocol was used, in which the reduction step was not performed, and the so-called BIOG-CRL-CuNPs-2.

### Enzymatic hydrolysis of 4-nitrophenyl propionate (pNPP)

This assay was performed by measuring the increase in the absorbance at 348 nm produced by the release of p-nitrophenol in the hydrolysis of 0.4 mM (pNPP) in 25 mM sodium phosphate buffer at pH 7 and 25 °C. To initialize the reaction, 3 mg of solid was added to 5 mL of substrate solution, measuring the absorbance at different times. In the case of lipase solution, 20  $\mu\text{L}$  of enzyme was added to 2.5 mL of substrate solution. The assay is performed in 4.5 mL of plastic cuvette, containing 2.5 mL 25 mM sodium phosphate buffer adding 20  $\mu\text{L}$  of 50 mM pNPP solution in acetonitrile. The solution was stirring to homogenise the solution and then 20  $\mu\text{L}$  of enzyme in solution or suspension (from solid) was added. The hydrolytic process was followed using a JASCO spectrophotometer, measuring the absorbance at different times of reaction, or in continue in the kinetic program if the equipment presented a magnetic stirrer. The enzymatic activity was expressed in specific activity per amount of protein (U/mg). The specific activity (U/mg) was calculated using the following equation:

$$U(\mu\text{mol} \cdot \text{min}^{-1} \cdot \text{mg}^{-1}) = \frac{\Delta\text{Abs}/\text{min} \cdot V}{\epsilon \cdot \text{mg}_{\text{protein}}}$$

where the molar extinction coefficient ( $\epsilon$ ) used was 5.15 mL/ $\mu\text{mol} \cdot \text{cm}$ , and mg of enzyme.

### Metallic catalytic reduction of 4-nitrophenol (pNP) to 4-aminophenol (pAP)

p-Nitrophenol (pNP) was dissolved in 2 mL of distilled water at to 1–10 mM concentration. Then,  $\text{NaBH}_4$  (40 mM) was added to the solution. After this addition, the light-yellow solution changes to a strong yellow colour, generating the formation of 4-nitrophenolate ions (substrate UV-peak undergoes to an immediate shift from 317 to 400 nm). After 30 seconds, 10 mg of catalyst were added under gentle stirring at room temperature in an orbital shaker. The reaction progress was monitored by taking out an aliquot of the solution (0.1 mL) at different times, diluting it with distilled water (2 mL) and measuring the absorption spectrum between 500 and 300 nm in a quartz cuvette.

## Synthesis of 3 from peracetylated glucose (1) catalysed by BIOG-CRL-CuNPs hybrids

$\alpha$ -D-glucose pentaacetate (25 mg) (1) was dissolved in 10 mL of 50 mM sodium acetate buffer at pH 4.8, containing in 20% of ACN (v/v). Then, 500  $\mu$ L of H<sub>2</sub>O<sub>2</sub> and 750 mg of catalyst were added. The reaction was followed by TLC and HPLC analysis at different times and room temperature. For the TLC measurement, hexane: ethyl acetate (1:1) was used as eluent. The products were detected by spraying the plate completely with a 10% (v/v) solution of H<sub>2</sub>SO<sub>4</sub> in methanol and on a hot plate where light brown spots will appear on the surface of the plate. The HPLC conditions were an isocratic mixture of 70:30 water:ACN as mobile phase, UV detection at 215 nm, and a flow rate of 1 mL/min. Under these conditions, retention times of  $\alpha$ -D-glucose pentaacetate (1),  $\alpha$ -6-OH (2) and product 3 were 16.5, 5.5 and 2.5 min, respectively.

For product isolation, after reaction complete, the product was separated from the catalyst BIOG-CRL-CuNPs-1) by centrifugation and the supernatant (aqueous phase) was transferred to a 250 ml separator funnel and the aqueous layer was extracted with ethyl acetate (9 $\times$ 20 ml). Subsequently, the organic layer was dried by adding about 1.5 g of anhydrous sodium sulphate. Shake gently for 5 min, filter the mixture by gravity through a fluted filter paper in a funnel to remove sodium sulphate, and collect the filtrate in a 250 ml round bottom flask. Evaporate the solvent using a rotary evaporator at 40 °C under vacuum aspirator (200 mbar) to obtain the product. <sup>1</sup>H NMR (400.13 MHz, D<sub>2</sub>O, 25 °C):  $\delta$  = 6.17 (d, J = 3.6 Hz, 1H, H-2), 5.27 (t, J = 10 Hz, 1H, H-4), 5.03 (dd, J = 10 Hz, J = 4 Hz, 1H, H-3), 4.28, 4.04 (AB part of an ABX spin system, 2H, CH<sub>2</sub>-H6a,b), 3.78 (dd, J = 10 Hz, J = 9.2 Hz, 1H, H-5), 2.15 (s, 3H, Ac), 2.06 (s, 3H, Ac), 2.04 (s, 3H, Ac). <sup>13</sup>C NMR (100.61 MHz, D<sub>2</sub>O, 25 °C):  $\delta$  = 174.23 (2 C collapsed, C=O), 172.18 (C=O), 89.16 (C-2), 71.73 (C-6), 20.30 (Me), 20.18 (2 C collapsed, Me). No more <sup>13</sup>C could be determined. <sup>13</sup>C chemical shifts were obtained from edited-HSQC and HMBC 2D <sup>1</sup>H-<sup>13</sup>C correlation spectra. Despite large accumulation trials, no signals were found in the <sup>13</sup>C APT spectrum.

## Acknowledgements

The authors thank the support of the Spanish National Research Council (CSIC) (projects PIE 201980E081 and MCIN/AEI/10.13039/501100011033, Project No. PID2019-106394GB-I00/AEI/10.13039/501100011033), and also by the Gobierno de Aragón-FSE (Spain, research group Aminoácidos y Péptidos E19\_20R). The authors also wish to acknowledge the funding from European Commission, project "Twinning for intensified enzymatic processes for production of prebiotic-containing functional food and bioactive cosmetics" grant no. 101060130, HORIZON-WIDERA-2021-ACCESS-02-01. We also thank Dr. Martinez from Novozymes for the gift of CALB and TLL enzymes. The Authors would like to acknowledge networking support by the COST Action CA18132 (GlycoNanoProbes).

## Conflict of Interest

The authors declare no conflict of interest.

## Data Availability Statement

The data that support the findings of this study are available from the corresponding author upon reasonable request.

**Keywords:** bifunctional catalyst · carbohydrate chemistry · chemoenzymatic reaction · enzymes · metal nanoparticles

- [1] P. Valverde, A. Arda, N.-C. Reichardt, J. Jiménez-Barbero, A. Gimeno, *MedChemComm* **2019**, *10*, 1678–1691.
- [2] B. Palitzsch, N. Gaidzik, N. Stergiou, S. Stahn, S. Hartmann, B. Gerlitzki, N. Teusch, P. Flemming, E. Schmitt, H. Kunz, *Angew. Chem. Int. Ed.* **2016**, *55*, 2894–2898; *Angew. Chem.* **2016**, *128*, 2944–2949.
- [3] R. Hevey, *Pharmaceuticals* **2019**, *12*, 55.
- [4] S. E. Kurhade, P. Ross, F. P. Gao, M. P. Farrell, *ChemBioChem* **2022**, *23*, e202200266.
- [5] X. Yang, H. Yu, X. Yang, A. S. Kooner, Y. Yuan, B. Luu, X. Chen, *ChemCatChem* **2022**, *21*, e202101498.
- [6] G. L. Thanh, et al., *J. Org. Chem.* **2010**, *75*, 197.
- [7] K. Kimura, I. Yoshioka, (2019). *Gluconic and Itaconic Acids*. *Compr. Biotechnol.* **3** (3), 166–171. (Third Edition). doi:10.1016/B978-0-444-64046-8.00158-0.
- [8] M. B. Li, J. E. Bäckvall, *Acc. Chem. Res.* **2021**, *54*, 2275–2286.
- [9] D. Kracher, R. Kourist, *Curr. Opin. Green Sustain. Chem.* **2021**, *32*, 100538.
- [10] Y. Ge, F. Ye, J. Yang, A. Spannenberg, H. Jiao, R. Jackstell, M. Beller, *Angew. Chem. Int. Ed.* **2021**, *60*, 22393–22400; *Angew. Chem.* **2021**, *133*, 22567–22574.
- [11] X.-Y. Chai, H.-B. Xu, L. Dong, *Chem. Eur. J.* **2021**, *27*, 13123–13127.
- [12] a) E. B. Bauer, *Org. Biomol. Chem.* **2020**, *18*, 9160–9180; b) V. Aumala, F. Mollerup, E. Jurak, F. Blume, J. Karppi, A. E. Koistinen, E. Schuiten, M. Voß, U. Bornscheuer, J. Deska, E. R. Master, *ChemSusChem* **2019**, *12*, 848–857.
- [13] a) R. Schoevaart, T. Kieboom, *Tetrahedron Lett.* **2002**, *43*, 3399–3400; b) M. Makkee, A. P. G. Kieboom, H. Van Bekkum, J. A. Roels. *J. Chem. Soc. Chem. Commun.* **1980**, 930–931.
- [14] F. Rudroff, M. D. Mihovilovic, H. Gröger, R. Snajdrova, H. Iding, U. T. Bornscheuer, *Nat. Catal.* **2018**, *1*, 12–22.
- [15] A. D. Liang, J. Serrano-Plana, R. L. Peterson, T. R. Ward, *Acc. Chem. Res.* **2019**, *52*, 585–595.
- [16] C. Garcia-Sanz, A. Andreu, B. de las Rivas, A. I. Jiménez, A. Pop, C. Silvestru, E. P. Urriolabeitia, J. M. Palomo, *Org. Biomol. Chem.* **2021**, *19*, 2773–2783.
- [17] K. P. Gustafson, T. Görbe, G. de Gonzalo-Calvo, N. Yuan, C. L. Schreiber, A. Shchukarev, C.-W. Tai, I. Persson, X. Zou, J. E. Bäckvall, *Chem. Eur. J.* **2019**, *25*, 9174–9179.
- [18] R. Chapman, M. H. Stenzel, *J. Am. Chem. Soc.* **2019**, *141*, 2754–2769.
- [19] a) K. Engström, E. V. Johnston, O. Verho, K. P. J. Gustafson, M. Shakeri, C.-W. Tai, J.-E. Bäckvall, *Angew. Chem. Int. Ed.* **2013**, *52*, 14006–14010; *Angew. Chem.* **2013**, *125*, 14256–14260; b) T. Görbe, K. P. J. Gustafson, O. Verho, G. Kervefors, H. Zheng, X. Zou, E. V. Johnston, J.-E. Bäckvall, *ACS Catal.* **2017**, *7*, 1601–1605; c) K. P. J. Gustafson, T. Görbe, G. de Gonzalo-Calvo, N. Yuan, C. L. Schreiber, A. Shchukarev, C.-W. Tai, I. Persson, X. Zou, J.-E. Bäckvall, *Chem. Eur. J.* **2019**, *25*, 9174–9179; d) L. Deiana, A. A. Rafi, V. R. Naidu, C.-W. Tai, J.-E. Bäckvall, A. Córdoba, *Chem. Commun.* **2021**, *57*, 8814–8817.
- [20] S. Gao, Y. Liu, L. Wang, Z. Wang, P. Liu, J. Gao, Y. Jiang, *ACS Catal.* **2021**, *11*, 5544–5553.
- [21] Y. Liu, P. Liu, S. Gao, Z. Wang, P. Luan, J. González-Sabín, Y. Jiang, *Chem. Eng. J.* **2021**, *420*, 127659.
- [22] H. Zhao, G. Liu, Y. Liu, X. Liu, H. Wang, H. Chen, J. Gao, Y. Jiang, *ACS Appl. Mater. Interfaces.* **2020**, *14*, 2, 2881–2892.
- [23] J. M. Naapuri, N. Losada-García, J. Deska, J. Palomo, *Nanoscale* **2022**, *14*, 5701–5715.
- [24] J. M. Palomo, *Chem. Commun.* **2019**, *55*, 9583–9589.
- [25] R. Benavente, D. Lopez-Tejedor, J. M. Palomo, *Chem. Commun.* **2018**, *54*, 6256–6259.
- [26] M. Filice, M. Marciello, M. P. Morales, J. M. Palomo, *Chem. Commun.* **2013**, *49*, 6876–6878.
- [27] R. Benavente, D. Lopez-Tejedor, M. P. Morales, C. Perez-Rizquez, J. M. Palomo, *Nanoscale* **2020**, *12*, 12917–12927.



- [28] M. Filice, N. Losada-Garcia, C. Perez-Rizquez, M. Marciello, M. P. Morales, J. M. Palomo, *Appl. Nano* **2021**, *2*, 1–13.
- [29] N. Losada-Garcia, A. Rodriguez-Otero, J. M. Palomo, *Catal. Sci. Technol.* **2020**, *10*, 196–206.
- [30] M. Filice, J. M. Guisan, M. Terreni, J. M. Palomo, *Nat. Protoc.* **2012**, *7*, 1783–1796.
- [31] G. Fernández-Lorente, Z. Cabrera, C. Godoy, R. Fernandez-Lafuente, J. M. Palomo, J. M. Guisan, *Process Biochem.* **2008**, *43*, 1061–1067.
- [32] H. Seelajaroen, A. Bakandritsos, M. Otyepka, R. Zboril, N. S. Sariciftci, *ACS Appl. Mater. Interfaces* **2020**, *12*, 250–259.
- [33] J. J. Zhang, F. Zhang, H. Yang, X. Huang, H. Liu, J. J. Zhang, S. Guo, *Langmuir* **2010**, *26*, 6083–6085.
- [34] N. Losada-Garcia, A. Berenguer-Murcia, D. Cazorla-Amoros, J. M. Palomo, *Nanomaterials* **2019**, *9*, 1344.

---

Manuscript received: December 20, 2022  
Revised manuscript received: March 6, 2023  
Accepted manuscript online: March 12, 2023  
Version of record online: April 5, 2023